ISSN: 1410-8917
Jurnal Kimia Sains & Aplikasi
e-ISSN: 2597-9914

Jurnal Kimia Sains dan Aplikasi 29 (2) (2026): 101-110

Jurnal Kimia Sains dan Aplikasi
Journal of Scientific and Applied Chemistry

Journal homepage: http://ejournal.undip.ac.id/index.php/ksa

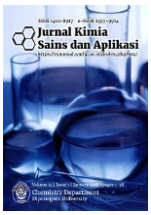

The Effect of Fe Pillaring and Mg Intercalating into Bentonite Structure

Dian Maruto Widjonarko *, Edi Pramono, Sentot Budi Rahardjo, Sayekti Wahyuningsih, Teguh Endah Saraswati

Department of Chemistry, Sebelas Maret University, Jalan Ir. Sutami 36A, Kentingan, Surakarta, Central Java, Indonesia

* Corresponding author: dianmaruto@staff.uns.ac.id

https://doi.org/10.14710/jksa.29.2.101-110

Article Info

Article history:

Received: 10th November 2025
Revised: 13th February 2026
Accepted: 15th February 2026
Online: 14th March 2026

Keywords:
basal spacing; bentonite; intercalation; modification; pillarization

Abstract

Bentonite clay particles, measuring less than 2 µm, comprise stacked layers of tetrahedral and octahedral units in a 2:1 configuration (T-O-T). These negatively charged layers were subsequently neutralized with cations. However, the exchange or modification of the cation affects its structure and properties. This study investigates the effect of Fe-ion pillaring on the bentonite layer and the intercalation of Mg ions into Fe-pillared bentonite via ion exchange. The materials were characterized using Scanning Electron Microscopy with Energy Dispersive X-ray Spectroscopy (SEM–EDX) to observe surface morphology and elemental composition, Particle Size Analyzer (PSA) to observe average size and size distribution of particle, Fourier-Transform Infrared Spectroscopy (FTIR) to identify the active site and layer structure, and X-ray Diffraction (XRD) to determine their structural and compositional changes. The results confirm the pillaring treatment effect on a higher average particle size of 469.3 nm, with a polydispersity index (PDI) of 0.495, compared to natural bentonite (414.8 nm and 0.586 nm, respectively). Meanwhile, the intercalating treatment showed a lower average particle size of 433.4 nm and a PDI value of 0.613. FTIR identified the silanol and siloxane functional groups, as well as the aluminosilicate layer. Pillaring by Fe_2O_3 increased the basal spacing of bentonite from 13.6 Å to 17.35 Å, as indicated by the shift of characteristic bentonite peaks to lower 2θ angles. However, intercalation by MgO into Fe-pillared bentonite actually slightly decreased the basal spacing to 15.16 Å. Meanwhile, Mg intercalation occurred within the interlayer of the aluminosilicate layer, resulting in a peak shift toward higher 2θ angles and an increase in crystallinity to 58.924%, compared with Fe-pillared bentonite (45.376%). This phenomenon is likely related to the presence of the Mg metal intercalant, which has basic properties and can attract the aluminosilicate sheets.

1. Introduction

Clay comprises colloid-sized particles rich in hydrated aluminum silicates, commonly originating from sedimentary or weathering processes. Mineralogically, it is dominated by hydrated phyllosilicates containing Si, O, OH, and H_2O, with elements such as Al, Mg, Fe, K, and Ca influencing their structure [1]. Clay particles (< 2 µm) form layered crystals of tetrahedral and octahedral units. The stacking of these units results in 1:1 (T-O) or 2:1 (T-O-T) structures. Negative charges, primarily arising from isomorphic substitution within the layers, contribute up to 90–95% of the total surface charge [2].

Based on their crystalline structures, clay minerals are classified into kaolinite, illite, and montmorillonite, with montmorillonite being the dominant component of bentonite. Formed from volcanic rock weathering, montmorillonite is a member of the smectite group that features a 2:1 layer structure composed of silica tetrahedra and an octahedral sheet of Al^{3+} or Mg^{2+} coordinated with oxygen and hydroxyl groups. This structure hosts exchangeable cations, typically Na^+ or

Ca^{2+}, between the layers. Bentonite exhibits a fine particle size, a high surface area, notable cation exchange capacity, swelling ability, and strong interaction with both organic and inorganic compounds [3, 4, 5].

Bentonite is a 2:1 clay mineral comprising two silica tetrahedral sheets and a central alumina octahedral sheet, with interlayer water molecules that enable significant swelling and high cation exchange capacity. Despite its utility as a catalyst [6, 7] and an adsorbent [8, 9], natural bentonite has limitations due to the presence of impurities and a narrow interlayer spacing [10]. These drawbacks can be addressed through modification techniques, particularly pillaring [11]. Cation exchange with metal species, followed by oxidation, leads to the formation of metal oxide pillars (e.g., Al, Zr, Ti, Fe, Cr) between the layers [12, 13, 14]. These pillars stabilize the interlayer structure, increase surface area, and enhance thermal and chemical stability. The pillaring process introduces permanent inorganic frameworks that not only expand the interlayer distance but also improve bentonite's performance in adsorption and catalysis.

The interlayer space of bentonite can accommodate various materials, with its exchangeable cations acting as the driving force for intercalation. Intercalation involves inserting atoms or molecules into the interlayer galleries without disrupting the clay's layered structure. These intercalants, typically cationic species, replace loosely bound native cations, such as Na^+, K^+, Ca^{2+}, and even transition-metal ions, via cation-exchange processes [15]. This modification not only increases access to internal pore spaces but also introduces new active sites between layers [8]. Magnesium, as an earth alkaline metal, has an intrinsic basicity and surface chemical properties. MgO is a well-known basic oxide that can introduce Lewis base sites, thereby modulating the surface acidity–basicity balance of the pillared bentonite [16].

Previous studies have demonstrated that Fe–Al pillaring enhances bentonite's physicochemical properties, as indicated by an expanded interlayer spacing and a downward shift in XRD peaks, while maintaining structural integrity. Subsequent addition of CaO_2 enabled its use as a catalyst for H_2O_2 in degrading trichloroethylene in contaminated soil and groundwater [17]. Despite these advances, existing Fe–Al pillared clay systems predominantly emphasize interlayer expansion and surface area enhancement, while the potential of post-pillaring modification to fine-tune interlayer chemistry and structural ordering remains underexplored [11]. In particular, the role of secondary alkaline-earth species introduced after pillaring has received limited attention. In this study, a sequential modification strategy is proposed in which Fe-pillaring is first employed to stabilize and expand the bentonite interlayers, followed by Mg-based intercalation as a post-pillaring functional modification, potentially effective for dye adsorption [16].

2. Experimental

2.1. Materials

The materials used in this experiment included raw bentonite sourced from Pacitan, East Java, Indonesia; silver nitrate ($AgNO_3$); ferric chloride hexahydrate ($FeCl_3{\cdot}6H_2O$); magnesium chloride hexahydrate ($MgCl_2{\cdot}6H_2O$); hydrochloric acid (HCl, 37%); hydrogen peroxide (H_2O_2, 30%); and ammonia solution (25%). All chemical reagents were of analytical grade and obtained from Merck. Additional materials included Whatman No. 41 filter paper and aluminum foil. The equipment used in this study included a non-mercury glass thermometer (Iwaki), dropper pipettes, a Buchner filtration setup, standard laboratory glassware (Pyrex), universal pH paper (MColorpHast), mortar and pestle, an analytical balance (Fujitsu FSR-A320; max capacity: 300 g; readability: 0.001 g), a hotplate with magnetic stirrer, muffle furnace, and several characterization instruments.

2.2. Procedures

2.2.1. Bentonite Preparation

Bentonite was prepared using the sedimentation method. The bentonite was dispersed in distilled water at a 1:10 (w/v) ratio, followed by continuous stirring for 30 minutes. To remove magnetic impurities, a magnet was placed underneath the beaker containing the suspension and left undisturbed for 7 days. During this period, impurities were attracted and settled at the bottom of the beaker due to magnetic forces. The purified bentonite was then separated from the accumulated impurities by decantation. Finally, the bentonite was dried overnight at 90°C.

2.2.2. Pillarization with Fe Species

Fe-pillared bentonite was synthesized via a pillarization method. A pillaring solution was prepared by slowly adding 400 mL of 0.2 M NaOH to 200 mL of 0.2 M $FeCl_3{\cdot}6H_2O$ under stirring until the pH reached 4, then stirring for 4 hours at room temperature. Separately, 20 g of purified bentonite was dispersed in 200 mL of distilled water (1:10 w/v), homogenized manually, and then stirred mechanically for 2 hours. Subsequently, 100 mL of the pillaring solution was added dropwise to the bentonite suspension, which was stirred continuously for 18 hours. The resulting mixture was filtered, and the solid was washed with distilled water until no Cl^- was detected (as determined by $AgNO_3$). The sample was dried at 75°C overnight, calcined at 400°C for 2 hours, then ground and sieved through a 200-mesh screen.

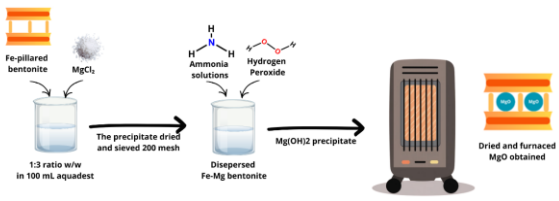

Figure 1. Schematic diagram for Mg intercalated onto pillared bentonite

2.2.3. Intercalation with Mg Species

The Mg-based intercalation process was initiated by inserting Mg^{2+} ions into the Fe-pillared bentonite. A total of 3 g of Fe-pillared bentonite was mixed with 9 g of $MgCl_2$ (1:3 ratio w/w) in a 100 mL beaker, followed by the addition of 10 mL of distilled water and 1 mL of HCl. The resulting mixture was stirred and subsequently filtered using a vacuum Büchner funnel. The obtained solid was dried at 120°C and sieved through a 200-mesh standard sieve. Next, 7 mL of $NH_3{\cdot}H_2O$ was added to the mixture, followed by the dropwise addition of 7 mL of excess H_2O_2 into 20 mL of cold Fe–Mg^{2+}-intercalated bentonite suspension under continuous stirring. H_2O_2 was added to ensure complete oxidation of residual Fe^{2+} to Fe^{3+}, thereby stabilizing the iron oxide pillars. This step was carried out inside a fume hood. The appearance of a white coloration indicated the formation of magnesium hydroxide, $Mg(OH)_2$, which is expected to undergo dehydration to MgO upon subsequent thermal treatment. The final product was then dried at 80°C and calcined at 400°C for 3 hours. Figure 1 shows the schematic diagram of MgO intercalated onto pillared bentonite.

2.3. Characterization of Modified Bentonite

2.3.1. Morphology and Elemental Constituent Characterization

The morphological and elemental composition of the samples was examined using Scanning Electron Microscopy coupled with Energy-Dispersive X-ray spectroscopy (SEM-EDX; JEOL NeoScope JCM0700). The analysis was conducted at an accelerating voltage of 15.0 kV, with magnifications of 500×, 1000×, 5000×, and 10,000×. Elemental mapping was performed to identify and localize the distribution of dominant metal elements. The samples analyzed included Fe-pillared bentonite and Fe-Mg-intercalated bentonite.

2.3.2. Particle Size Characterization

The particle size distribution of bentonite was determined using a particle size analyzer (PSA) (Malvern Zetasizer Nano ZS Zen 3000). Sample preparation involved dispersing the bentonite powder in deionized water to obtain a homogeneous suspension. The analysis was performed under liquid conditions to ensure a clear and well-dispersed system prior to measurement. The samples analyzed included Fe-pillared bentonite and Mg-intercalated Fe-pillared bentonite.

2.3.3. Functional Group Characterization

Fourier Transform Infrared (FTIR) analysis of the bentonite samples was performed using the KBr pellet method. The spectra were recorded in the range of 400–4000 cm^{-1} using a Shimadzu IR-Prestige21 FTIR spectrophotometer. The analyzed samples included purified bentonite, Fe-pillared bentonite, and Fe-pillared bentonite further intercalated with Mg species.

2.3.4. Composition and Crystalline Characterization

The crystalline structure of the bentonite samples was characterized by X-ray diffraction (XRD) using an X'Pert PRO PANalytical diffractometer equipped with a Cu Kα radiation source (λ = 1.5406 Å). The instrument operated at 40 kV and 30 mA. Diffraction patterns were recorded over a 2θ range of 5°–90°. The analyzed samples included Fe-pillared bentonite and Fe-pillared bentonite further intercalated with Mg species. Then, the crystallinity of bentonite was measured by Equation (1) after deconvolution of the diffractogram with OriginLab.

$$Crystallinity\ (\%) = \frac{Ac}{(Ac+Aa)} \times 100\% \quad (1)$$

Where, Ac is the area of the crystalline peak, and Aa is the area of the amorphous in the XRD diffractogram.

3. Results and Discussion

3.1. Bentonite Preparation

The prepared bentonite samples were characterized using SEM to observe morphological bulk features. Figure 2 shows that SEM analysis of natural bentonite reveals a thick, flaky structure with a coarse surface texture, attributed to the presence of impurity minerals. Following the purification process, bentonite retains its flaky morphology but exhibits improved surface characteristics, including flatter surfaces, clearer particle boundaries, enhanced dispersion, and visible pores or cavities [18]. The purification also reduces surface roughness, reflecting a decrease in impurities. Furthermore, bentonite generally shows a non-homogeneous particle distribution due to variations in grain size within its layered structure [19]. Meanwhile, particle size analysis of natural bentonite revealed an average particle size of 414.8 nm, with a particle size distribution of 0.586 nm. EDX analysis (Table 1) shows the elemental distribution in natural bentonite. Pacitan bentonite contains higher Al and Si than Iraqi natural bentonite reported by Jawad et al. [20].

The ratio of Si: Al: O is approximately 2:1:5, which is ideal for bentonite. The data indicate that the analyzed minerals belong to the (alumino)silicate class, where negatively charged layers are balanced by exchangeable cations such as Na, Mg, and Ca. In addition, the presence of C, O, and Ca suggests the occurrence of carbonate minerals.

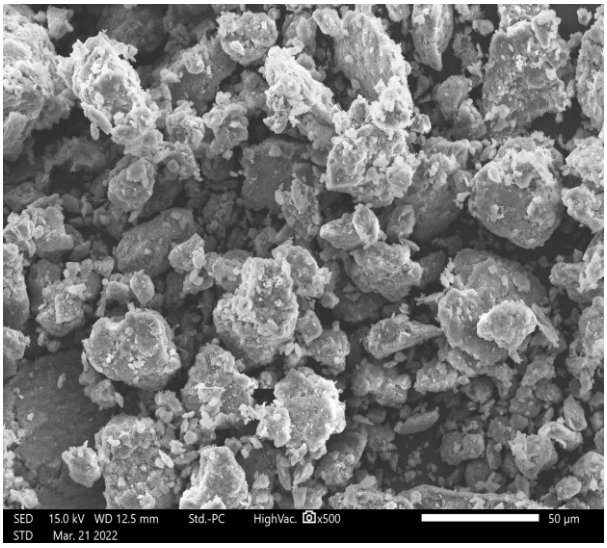

Figure 2. SEM image of natural bentonite

Table 1. Element distribution of natural bentonite

Element	Mass (%) w/w
C	6.22
O	54.97
Na	2.85
Mg	1.88
Al	10.24
Si	23.15
Ca	0.69

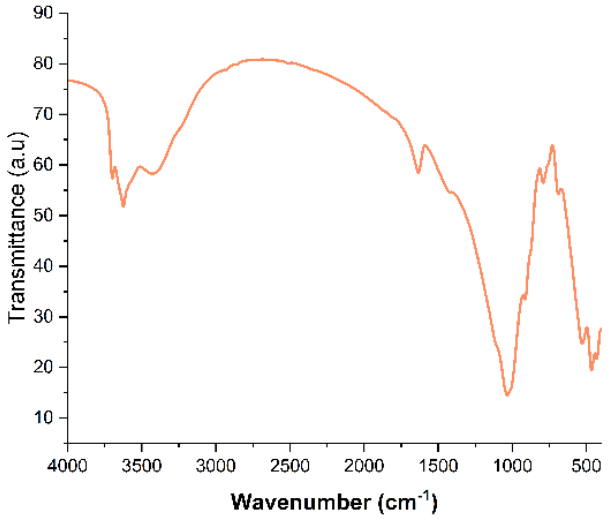

Figure 3. FTIR spectrum of natural bentonite

On the other hand, the FTIR spectrum (Figure 3) shows absorption bands corresponding to Si–O/Al–O and Si–O–Si/Si–O–Al bonds. The Si–O groups include Si–OH (silanol), which are acidic in nature because they can release H^+ and readily undergo cation exchange. Exchangeable cations such as Ca^{2+}, Mg^{2+}, and particularly Na^+ enable the material to bind various molecules. Meanwhile, Si–O–Si (siloxane) groups form part of the silicate sheet structure. Further details on the absorption bands observed in the FTIR spectrum of natural bentonite are presented in Table 2. However, the presence of carbonate minerals is not clearly indicated in the FTIR spectrum, as the characteristic strong absorptions around 1400–1500 cm^{-1} and 870–880 cm^{-1} are not distinctly observed.

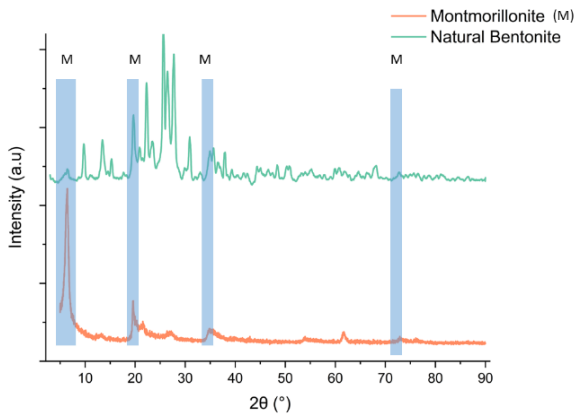

Figure 4. XRD diffractogram of natural bentonite and montmorillonite (RRUFF R110052)

Table 2. FTIR peaks of natural bentonite

Functional Group	Wavenumber (cm^{-1})	Reference wavenumber (cm^{-1})	Ref.
–OH group	3645	3628	[21]
O–H stretching	3536	3525	[22]
O–H stretching	3433	3428	[23]
O–H bending	1634	1639	[21, 24]
Si–O–Si/Si–O–Al	1047	1051	[24]
Si–O quartz and silica	796	798	[21]
Si–O–Al stretching	527	524	[23]
Si–O bending and Fe–O stretching	473	473	[21]

The XRD data of the natural bentonite sample (Figure 4) reveal multiple diffraction peaks, confirming its heterogeneous composition. Comparison with the standard montmorillonite reference (RRUFF R110052) confirms montmorillonite as the dominant phase, evidenced by peaks at 2θ = 6.27°, 19.51°, 34.74°, and 72.9°. This result corresponded with the findings reported in [25]. However, additional peaks indicate the presence of basal spacing of natural bentonite around 13.6 Å (6.27°) and of impurities, including quartz (20.76°, 26.66°), muscovite (27.98°), and hematite (~50°, 59°) with crystallinity of 34.750 %. Table 3 shows the mineral composition of natural bentonite. These findings align with typical bentonite mineralogy, where montmorillonite coexists with non-clay minerals due to natural geological processes [26].

The XRD analysis of natural bentonite shows diffraction peaks corresponding to the crystallographic planes of montmorillonite and associated impurities. The basal spacing (d_{001}) of the montmorillonite is approximately 13.6 Å. The characteristic (110) plane of montmorillonite appears at 19.51° (2θ), while the (124) plane is observed at 34.74° (2θ), confirming the presence of well-ordered smectite layers. A peak at 26.66° (2θ) corresponds to the (210) reflection of quartz (SiO_2), indicating its presence as a common impurity in the bentonite matrix. These reflections indicate that natural bentonite consists mainly of montmorillonite with crystalline quartz, reflecting its geological origin and suggesting that purification may be required depending on its intended application [27].

Table 3. Minerals in natural bentonite

Mineral	Composition (%)
Montmorillonite	47.74
Hematite	20.80
Quartz	23
Muskovite	8.46

3.2. Pillared Bentonite

The pillared bentonite samples were systematically characterized using a suite of analytical techniques. SEM coupled with EDX provided simultaneous morphological examination and elemental composition mapping. Particle size distribution profiles, including the average particle size and polydispersity index (PDI), were quantified through PSA. FTIR spectroscopy identified modifications in functional groups and bonding configurations. XRD analysis revealed changes in the crystallographic structure and interlayer spacing. This multi-technique approach comprehensively evaluates the physicochemical alterations induced by pillarization and intercalation processes.

Figure 5(a) shows the SEM image of Fe-pillared bentonite, revealing a layered, porous morphology characteristic of modified clay. Elemental mapping (Figure 5(b)) confirms the incorporation of Fe (green) into the bentonite matrix, shown by its homogeneous distribution with Si (red) and Na (blue). The coexistence of these elements suggests that the pillaring process preserved the aluminosilicate layers while introducing Fe species, likely as iron oxides or hydroxides, within the interlayer spaces. This modification is expected to enhance the bentonite's catalytic and adsorption properties due to an increased surface area and the active sites provided by the Fe pillars [11]. Figure 5(c) shows Mg-intercalated bentonite with a more compact, aggregated structure than the Fe-pillared variant. Elemental mapping (d) shows Mg (blue) distributed with Si (red) and residual Fe (green), indicating effective intercalation of Mg ions into the bentonite layers. The elemental distribution is homogeneous, suggesting the formation of a cation-exchanged structure [28].

In addition to morphological examination, the successful modification of bentonite was further verified through PSA. This technique provides quantitative evidence of structural alterations by measuring changes in average particle size and polydispersity index, offering complementary data to the morphological observations from SEM analysis.

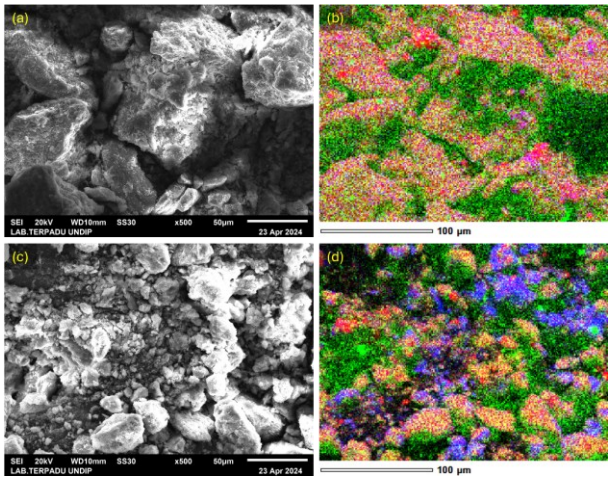

Figure 5. (a, b) SEM images and EDX mapping of pillared bentonite, and (c, d) SEM images and EDX mapping of intercalated bentonite

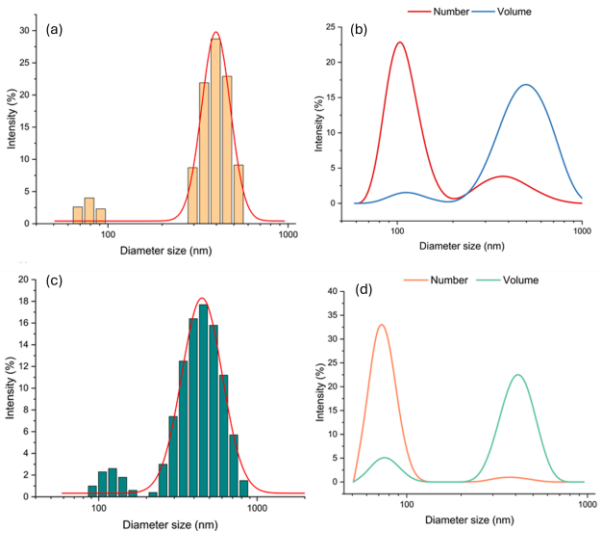

Figure 6. a) particle size distribution of pillared bentonite, (b) Correlation between number and volume in pillared bentonite, (c) particle size distribution of intercalated bentonite, (d) Correlation between number and volume in intercalated bentonite

Figure 6 provides a comprehensive comparison between Fe^{3+}-(a and b) and Mg^{2+}-intercalated bentonite (c and d). The intensity-based histograms display the relative frequency of particle size distribution, while the number–volume correlation plots further elucidate the dispersion characteristics within the samples. The average particle size of pillared bentonite was recorded at 469.3 nm, whereas intercalated bentonite exhibited a slightly smaller average size of 433.4 nm. Interestingly, this result contrasts with the distribution curves, in which intercalated bentonite shows a narrower, monomodal peak within the 100–200 nm range, while pillared bentonite displays a broader, bimodal distribution extending beyond 400 nm. On the other hand, the big difference in average particle size between natural and modified bentonite occurred because particle sizes reflect the apparent size of particle aggregates under dispersion conditions.

Natural bentonite typically exists as large tactoids composed of strongly stacked montmorillonite platelets, resulting in micron-scale aggregate sizes. Fe pillaring expands the interlayer spacing and weakens inter-platelet interactions, while subsequent Mg-based intercalation and alkaline treatment further enhance surface charge heterogeneity and electrostatic repulsion. These combined effects promote partial delamination and improved dispersion, leading to much smaller apparent particle sizes in the nanometer range. Therefore, the observed size reduction is attributed to changes in aggregation state rather than primary particle size.

This discrepancy can be attributed to the different physical interactions introduced during modification. In pillared bentonite, the insertion of Fe^{3+} polycations, followed by thermal treatment, leads to the formation of metal oxide pillars that permanently fix the smectite layers [29]. This process often causes interparticle bridging and agglomeration, particularly in the volume-based analysis, which tends to be weighted heavily toward

larger particles. As a result, although smaller particles are still present, the calculated average size is skewed by the presence of larger agglomerates, resulting in a higher mean diameter. Conversely, intercalation with Mg^{2+} predominantly involves ion exchange within the interlayer space without inducing significant structural rigidity or thermal condensation [30]. This leads to better particle dispersion and a more homogeneous particle size distribution, as evident in both number- and intensity-based plots. The smaller mean size of intercalated bentonite reflects the effective exfoliation and reduction of aggregation, which can enhance surface accessibility and interlayer diffusion, critical parameters in adsorption and catalytic applications.

Integrating the PSA data with the average particle size and PDI (Figure 7) provides a clearer understanding of the effects of modification on bentonite structure. After pillaring with Fe^{3+}, the average particle size increased to 469.3 nm, while the PDI decreased to 0.495, suggesting that although the particles tend to agglomerate due to the formation of oxide pillars, the distribution becomes more uniform. Mechanistically, the formation of rigid Fe_2O_3 pillars promotes interlayer fixation and particle–particle bridging, leading to controlled agglomeration rather than random clustering. This behavior is consistent with SEM images, which show compact, stacked platelet aggregates with relatively homogeneous morphology. This aligns with the volume-based distribution data, which shows that pillared bentonite shifts toward larger particle populations. The stabilization of the structure through thermal treatment during pillaring likely contributes to the reduced polydispersity, despite the presence of larger aggregates [31].

In contrast, intercalated bentonite exhibited a lower average particle size (433.4 nm) but a higher PDI (0.613) than the pillared sample. This combination of smaller mean size and higher PDI reflects a transition from agglomeration-dominated behavior (pillaring) to exfoliation-dominated behavior (intercalation). This behavior suggests that while Mg^{2+} intercalation promotes better dispersion and exfoliation at the microscopic level, it also introduces greater particle-size variation due to the dynamic ion-exchange process, which lacks structural fixation, such as pillaring. The presence of both smaller exfoliated sheets and occasional agglomerates results in a higher PDI.

Overall, both modifications (pillaring and intercalation) successfully altered the physical characteristics of natural bentonite. Pillaring enhanced structural regularity and reduced size variation, while intercalation improved particle dispersion. Although Mg intercalation reduces the average particle size, the PDI increases, indicating a broader size distribution rather than poorer dispersion. This arises from the non-uniform nature of Mg intercalation, which produces a mixture of highly delaminated fine particles and partially stacked aggregates. This structural heterogeneity is directly observed in SEM micrographs, which reveal thinner, more dispersed plate-like features alongside irregular agglomerates. Furthermore, Mg^{2+} hydrolysis under alkaline conditions introduces surface-chemical heterogeneity, promoting both electrostatic repulsion and localized reaggregation. Consequently, the system exhibits a smaller mean particle size but increased size heterogeneity, reflected in the higher PDI. Similar behavior has been reported for Mg-modified and post-pillared clay systems.

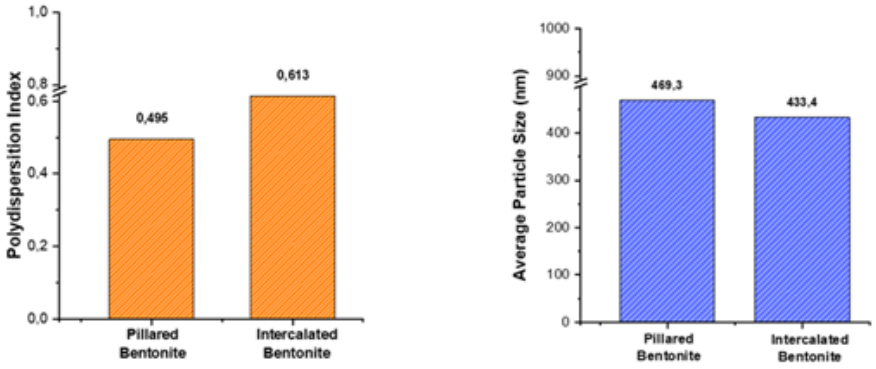

Figure 7. (a) Comparison of average particle size, (b) Comparison of polydispersity index of pillared and intercalated bentonite

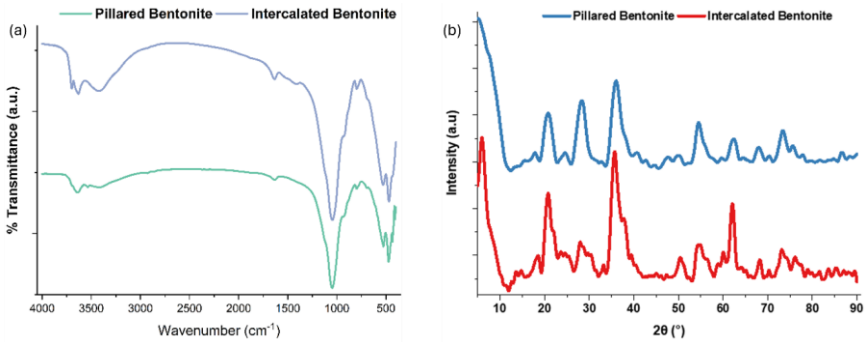

Figure 8. (a) FTIR spectra and (b) XRD diffractogram of pillared and intercalated bentonite

Table 4. FTIR spectra of Mg intercalated pillared bentonite

Wave number (cm^{-1})	Functional group
3698	OH bending
3631	H-OH stretching
3423	H-OH stretching
1635	H_2O
1410	Peroxide (O-O)
1044	Si-O-Si
797	Si-O quartz and silica
528	Si-O-Al stretching
469	Mg-O, Fe-O

On the other hand, Figure 8a shows that the success of Fe-pillaring is confirmed by the presence of Fe–O bonds at 473 cm^{-1} in the FTIR spectrum. The spectrum exhibits characteristic montmorillonite peaks, including hydroxyl stretching vibrations at 3645 cm^{-1} (attributed to Al–Al–OH and Al–Mg–OH in octahedral sheets) and 3536 cm^{-1} (associated with 2:1 layer OH stretching). A broad absorption band at 3433 cm^{-1} suggests surface-bound H_2O or OH stretching, further supported by the H– O–H bending mode at 1634 cm^{-1}. The OH groups may originate from both interlayer water and structural hydroxyls in the octahedral sheet (Al–OH). The Si–O–Si asymmetric stretching vibration appears at 1047 cm^{-1}, while a shift from 1038 cm^{-1} to 1051 cm^{-1} [24] indicates Fe_2O_3 formation in the interlayer. Impurity phases, such as quartz (weak Si–O band at 796 cm^{-1}), are present in trace amounts. Additional bands at 527 cm^{-1} (Si–O–Al) and 473 cm^{-1} (Fe–O–Si) further corroborate the pillared structure. Moreover, the peak positions of the FTIR spectra of intercalated bentonite are shown in Table 4, compared with those reported in the previous study.

Table 4 highlights key differences between modified and pillared bentonite. A weak absorption band at 1410 cm^{-1} in the modified sample suggests peroxide (–O–O–) formation, consistent with Mg oxide synthesis from $MgCl_2$ and H_2O_2. This is supported by the Mg–O stretching vibration at 469 cm^{-1}. The spectrum of Mg oxide derived from $MgCl_2$ also displays bands at 3693 cm^{-1} and 3441 cm^{-1} (hydrated OH groups), 1638 cm^{-1} (H_2O bending), and 493 cm^{-1} (Mg–O), aligning with reported data [32].

The FTIR spectra reveal distinct interaction mechanisms between Fe- and Mg-modified bentonite and the clay framework. In Fe-pillared bentonite, shifts and intensity changes in the –OH stretching (3645–3428 cm^{-1}) and bending (~1635 cm^{-1}) bands indicate strong interactions between Fe species and interlayer hydroxyl groups, consistent with the formation of Fe–O–Al/Si linkages. The presence of Fe–O vibrations near 473 cm^{-1} further supports the anchoring of iron oxide pillars to the silicate layers. In contrast, Mg-intercalated bentonite exhibits broader –OH stretching bands (3698–3423 cm^{-1}) and a Mg–O vibration around 469 cm^{-1}, reflecting weaker, predominantly electrostatic interactions and increased hydroxyl heterogeneity. The persistence of the Si–O–Si (~1044 cm^{-1}) and Si–O–Al (~528 cm^{-1}) bands confirms that the silicate framework remains intact after both modifications. Overall, FTIR indicates that Fe modification induces stronger chemical bonding and structural fixation, whereas Mg modification primarily alters the hydration environment and interlayer chemistry without disrupting the clay lattice.

The pillaring of bentonite with Fe^{3+} cations induces significant modifications in its crystallographic structure, as evidenced by the shift of XRD peaks (Figure 8b) toward lower 2θ angles, particularly in the 5°–10° range, which is characteristic of montmorillonite. This shift indicates an expansion of the interlayer spacing (basal spacing, d_{001}) from 13.6 Å to 17.35 Å, resulting from the replacement of native cations (Na^+, Ca^{2+}) by larger and more highly hydrated Fe^{3+} cations. This process leads to the formation of a more rigid pillar structure and increased interlayer dimensions.

Theoretically, pillaring with transition-metal cations, such as Fe^{3+}, increases basal spacing through electrostatic interactions between the positively charged cations and the negatively charged aluminosilicate layers, as reported by [33, 34]. This phenomenon is often accompanied by a reduction in peak intensity due to a more disordered spatial arrangement and an increased amorphous character, as observed by Russamsi et al. [35]. Table 5 presents the diffraction peaks of bentonite and their corresponding mineral phases.

In addition to the expansion of d-spacing, the formation of metal oxide pillars (e.g., hematite, Fe_2O_3) within the bentonite matrix is confirmed by the appearance of additional XRD peaks at 2θ = 27.97°, 35.60°, and 54.66°, which correspond to the reference diffraction pattern of Fe_2O_3 (RRUFF ID: R070240). These peaks confirm the formation of pillar components, while other peaks (e.g., at 26.71° and 19.89°) correspond to quartz as a secondary mineral. According to Sisnayati et al. [36], natural bentonite exhibits dominant peaks at 20.64° and 26.68°, whereas pillared bentonite shows additional peaks after modification.

The formation of Fe_2O_3 in the interlayer is hypothesized to occur through the oxidation of diffused Fe^{3+} ions within bentonite pores, followed by redox reactions that produce stable Fe–O covalent bonds [37, 38]. These bonds arise from the hybridization of Fe 3d and O 2p orbitals, reinforcing the structural framework of bentonite.

Table 5. Peaks of pillared bentonite

2θ angle (°)	Mineral	Composition (%)
5.069; 19.896	Montmorillonite	45.64
26.714	Quartz	7.61
27.968	Muscovite	11.51
35.602; 50.13; 54.667	Hematite	35.24

Table 6. XRD peak analysis of Mg-intercalated bentonite

2θ angle (°)	Material	Composition (%)
5.827; 20.01	Montmorillonite	48.27
26.724	Quartz	5.83
35.768; 50.25; 54.14	Hematite	30.15
18.666; 38.034; 58.589	MgO_2	15.75

From a clay mineralogical perspective, Fe^{3+} pillaring stabilizes the bentonite structure by forming rigid Fe_2O_3 oxide pillars that maintain the expanded basal spacing from 13.6 Å to 17.35 Å and prevent layer collapse, as evidenced by the persistence of low-angle basal reflections in the XRD patterns. In contrast, Mg^{2+} intercalation does not introduce permanent pillars but modifies the interlayer environment by reducing interlayer water and promoting layer densification. This densification is reflected in the contraction of basal spacing to 15.16 Å relative to Fe-pillared bentonite, along with sharper XRD peaks, indicating improved layer stacking order and enhanced apparent crystallinity. Thus, although thermal stability is not directly evaluated, the observed XRD features suggest a more ordered, structurally stabilized Mg-intercalated system than natural bentonite.

Mg^{2+} intercalation also exhibits distinct structural characteristics. The XRD diffractogram shows a peak shift from 5.39° to 5.94°, indicating a decrease in basal spacing. This observation is consistent with findings reported in [39], where the presence of nanoparticles (e.g., Fe_3O_4) in the interlayer can induce structural densification by compressing interlayer distances. Additionally, Table 6 shows the composition of intercalated bentonite. The presence of MgO indicates the modification is successful. However, Mg^{2+} functions as an intercalating agent rather than a structural pillar, occupying the interlayer space and strengthening internal bonds through electrostatic interactions. The effects of intercalation are also reflected in peak broadening, indicating increased amorphous character and localized modifications in crystallinity [40].

Although Mg^{2+} does not form structural pillars like Fe^{3+}, its presence still influences the crystalline arrangement and surface properties of the modified bentonite. The slight decrease in basal spacing observed after Mg intercalation is associated with interlayer densification rather than structural collapse. The incorporation of compact Mg-based species reduces excess interlayer water and promotes more ordered stacking of clay layers. Consequently, an increase in apparent crystallinity is observed, as indicated by enhanced peak intensity and sharpening in the XRD pattern. Similar behavior has been reported in Mg-modified pillared clays, where improved structural ordering accompanies a moderate reduction in interlayer spacing [41, 42].

Increased basal spacing between bentonite aluminosilicate layers due to pillarization can improve its chemical and physical properties. The properties of catalytic activity, selectivity, adsorption capacity, diffusion, volume, and surface area increase due to the ease with which reactant molecules can access the catalyst, determining the size of reactant molecules, volume, and surface area of bentonite particles. Pillarization of bentonite with Fe compounds, followed by intercalation with Mg compounds, can increase the material's thermal stability. Bentonite pillared with Fe compounds (45.376%) has lower crystallinity than bentonite pillared with Fe and intercalated with Mg (58.924%). It can be estimated that the thermal stability of bentonite resulting from pillarization and intercalation is much better than that of pillared bentonite.

4. Conclusion

Pillaring bentonite with Fe increased the basal spacing, as indicated by the shift of characteristic bentonite peaks to lower 2θ angles, accompanied by a reduction in crystallinity. However, intercalation with Mg into Fe-pillared bentonite actually slightly decreased the basal spacing. Meanwhile, Mg intercalation within the interlayer of the aluminosilicate sheets resulted in a peak shift toward higher 2θ angles and an increase in crystallinity compared to Fe-pillared bentonite. This phenomenon is likely related to the presence of the Mg metal intercalant, which has basicity properties and can attract the aluminosilicate layers, thereby increasing bentonite crystallinity and decreasing the basal spacing. These characteristics will improve both adsorption and catalytic performance by making active surfaces more accessible and enabling interactions with larger molecules. Fe–Mg modified bentonite is best envisioned as a low-cost, thermally stable, multifunctional adsorbent–catalyst for water, soil, and emerging contaminant remediation.

Acknowledgement

This research was supported by the LPPM Universitas Sebelas Maret under contract number 194.2/UN27.22/PT.01.03/2024.

References

[1] Friedrich Ruttner, *Biogeography and taxonomy of honeybees*, Springer Science & Business Media, 2013,

[2] W. A. Deer, FRS, R. A. Howie, J. Zussman, *An Introduction to the Rock-Forming Minerals*, Mineralogical Society of Great Britain and Ireland, 2013, ^https://doi.org/10.1180/DHZ

[3] Babak Jaleh, Seyedeh Soheila Mousavi, Mohaddeseh Sajjadi, Mahtab Eslamipanah, Motahar Jafari Maryaki, Yasin Orooji, Rajender S. Varma, Synthesis of bentonite/Ag nanocomposite by laser ablation in air and its application in remediation, *Chemosphere*, 315, (2023), 137668 https://doi.org/10.1016/j.chemosphere.2022.137668

[4] Yue Hui, Qun Huan, Yue Hu, Zonghao Liu, Jiahao Lai, Shaofeng Wang, Xian Cao, Ziye Wang, Yantao Guo, Min Song, Permeability and adsorption mechanisms of surfactant and polymer modified bentonite in Pb(Ⅱ) and Cr(Ⅵ contaminated groundwater, *Separation*

and Purification Technology, 366, (2025), 132774 https://doi.org/10.1016/j.seppur.2025.132774

[5] Shima Barakan, Valeh Aghazadeh, Separation and characterisation of montmorillonite from a low-grade natural bentonite: using a non-destructive method, *Micro & Nano Letters*, 14, 6, (2019), 688-693 https://doi.org/10.1049/mnl.2018.5364

[6] Somayeh Heydari, Biosynthesis of the Ag Doped SnO_2 Nanorods Supported Bentonite Clay with Enhanced Photocatalytic Activity Against Crystal Violet Dye, *Journal of Inorganic and Organometallic Polymers and Materials*, 35, 3, (2025), 2162-2173 https://doi.org/10.1007/s10904-024-03411-x

[7] Fanbo Zeng, Jing Zhu, Feng Liu, Guoyu Zhang, Weirun Li, Wenye Li, Zhiwei Shang, Hong You, Shuxiao Wang, Zhipeng Li, Bentonite supported cobalt catalyst prepared by blending method for the catalytic oxidation of desulfurization by-product sulfite: Catalytic performance and mechanism, *Journal of Environmental Sciences*, 156, (2025), 584-595 https://doi.org/10.1016/j.jes.2025.02.032

[8] Gabriela Kamińska, Bhautik Dave, Augustine Nana Sekyi Appiah, Justyna Majewska, Exploitation of bentonite and halloysite fixed bed columns – Removal of organic micropollutants and microbiological regeneration, *Desalination and Water Treatment*, 322, (2025), 101113 https://doi.org/10.1016/j.dwt.2025.101113

[9] Mahmoud I. Eleraky, Taha M. A. Razek, Ibrahim W. Hasani, Yosri A. Fahim, Adsorptive removal of lead, copper, and nickel using natural and activated Egyptian calcium bentonite clay, *Scientific Reports*, 15, 1, (2025), 13050 https://doi.org/10.1038/s41598-025-95184-7

[10] Bayu Aditya Nugraha, Ariadne Lakshmidevi Juwono, Nino Rinaldi, Egi Agustian, Teuku Beuna Bardant, Reaction condition optimization of biodiesel from waste cooking oil using Ti-Zr pillared bentonite as a solid acid catalyst by cheminformatics approach, *AIP Conference Proceedings*, 2902, 1, (2023), 030003 https://doi.org/10.1063/5.0173616

[11] Samira M. Abdel-Azim, Noha A. K. Aboul-Gheit, Sherif A. Younis, Sahar M. Ahmed, Synergistic role of pillared bentonite with single and binary Fe/Al-polyoxocations on Pb(II) adsorption recovery from hard water under competitive and non-competitive effects, *Applied Clay Science*, 267, (2025), 107716 https://doi.org/10.1016/j.clay.2025.107716

[12] Egi Agustian, Ariadne L. Juwono, Nino Rinaldi, Adid Adep Dwiatmoko, Pillaring of bentonite clay with Zr, Ti, and Ti/Zr by ultrasonic technique for biodiesel production, *South African Journal of Chemical Engineering*, 45, (2023), 228-239 https://doi.org/10.1016/j.sajce.2023.06.001

[13] Seyed Heydar Mosavi Mirak, Seyedmehdi Sharifian, Fatemeh Esmaeili Khalil Saraei, Neda Asasian-Kolur, Bahram Haddadi, Christian Jordan, Michael Harasek, Titanium-Pillared Clay: Preparation Optimization, Characterization, and Artificial Neural Network Modeling, *Materials*, 15, 13, (2022), 4502 https://doi.org/10.3390/ma15134502

[14] Robert R. Widjaya, Nanda Saridewi, Alda A. Putri, Nino Rinaldi, Adid A. Dwiatmoko, Fe-Cr pillared clay as catalysts for the ethanol to gasoline conversion, *IOP Conference Series: Materials Science and Engineering*, 1011, 1, (2021), 012008 https://doi.org/10.1088/1757-899X/1011/1/012008

[15] Peter Bohác, Laure Delavernhe, Erik Zervas, Franz Königer, Rainer Schuhmann, Katja Emmerich, Cation exchange capacity of bentonite in a saline environment, *Applied Geochemistry*, 100, (2019), 407-413 https://doi.org/10.1016/j.apgeochem.2018.12.019

[16] C. Pighini, T. Belin, J. Mijoin, P. Magnoux, G. Costentin, H. Lauron-Pernot, Microcalorimetric and thermodynamic studies of CO_2 and methanol adsorption on magnesium oxide, *Applied Surface Science*, 257, 15, (2011), 6952-6962 https://doi.org/10.1016/j.apsusc.2011.03.040

[17] Mengbin Gu, Usman Farooq, Shuguang Lu, Xiang Zhang, Zhaofu Qiu, Qian Sui, Degradation of trichloroethylene in aqueous solution by rGO supported nZVI catalyst under several oxic environments, *Journal of Hazardous Materials*, 349, (2018), 35-44 https://doi.org/10.1016/j.jhazmat.2018.01.037

[18] Doaa Ahmed El-Nagar, Dalal Hereimas Sary, Synthesis and characterization of nano bentonite and its effect on some properties of sandy soils, *Soil and Tillage Research*, 208, (2021), 104872 https://doi.org/10.1016/j.still.2020.104872

[19] Zhao Zhang, Wen-Sheng Geng, Wei-Min Ye, Yong He, Wei Su, Qiong Wang, Yong-Gui Chen, Comparative study of hydro-mechanical behaviors of compacted bentonite powder and granular bentonite, *Journal of Rock Mechanics and Geotechnical Engineering*, 17, 3, (2025), 1757-1769 https://doi.org/10.1016/j.jrmge.2024.05.034

[20] Ali H. Jawad, Shihab Ezzuldin M. Saber, Ahmed Saud Abdulhameed, Ahlam M. Farhan, Zeid A. Alothman, Lee D. Wilson, Characterization and applicability of the natural Iraqi bentonite clay for toxic cationic dye removal: Adsorption kinetic and isotherm study, *Journal of King Saud University – Science*, 35, 102630 https://doi.org/10.1016/j.jksus.2023.102630

[21] Novia Arinda Pradisty, Riwandi Sihombing, Russell Francis Howe, Yuni Krisyuningsih Krisnandi, Fe (III) oxide-modified Indonesian bentonite for catalytic photodegradation of phenol in water, *Makara Journal of Science*, 21, 1, (2017), 25-33

[22] Dwiarso Rubiyanto, Nurcahyo Iman Prakoso, Khoirunnisa, Putwi Widya Citradewi, Gani Purwiandono, Suresh Sagadevan, Is Fatimah, Microwave-assisted synthesized porous clay heterostructure-Zn/Si from montmorillonite for citronellal conversion into isopulegol, *Materials Research Express*, 7, 10, (2020), 105006 https://doi.org/10.1088/2053-1591/abbda7

[23] Neway Belachew, Getahun Bekele, Synergy of Magnetite Intercalated Bentonite for Enhanced Adsorption of Congo Red Dye, *Silicon*, 12, 3, (2020), 603-612 https://doi.org/10.1007/s12633-019-00152-2

[24] Claudia Neriva Cromain, Karakterisasi Bentonit Terpilar Fe_2O_3 sebagai Adsorben, *UNESA Journal of Chemistry*, 5, 3, (2016),

[25] A. Seidi, M. Benhamou, D. Khalil, M. Aalaoul, M. Naciri Bennani, Elaboration and characterization of a natural bentonite-poly(ethylene glycol) composite: Development of an exact theoretical

study in function of the polymer-density, *Chemical Physics Impact*, 9, (2024), 100673 https://doi.org/10.1016/j.chphi.2024.100673

[26] Tatiana Koroleva, Victoria Krupskaya, Ekaterina Tyupina, Ivan Morozov, Pavel Kozlov, Boris Pokidko, Sergey Zakusin, Tatiana Zaitseva, Impacts of Impurity Removal Chemical Pretreatment Procedures on the Composition and Adsorption Properties of Bentonites, *Minerals*, 14, 8, (2024), 736 https://doi.org/10.3390/min14080736

[27] Raghavendra S. Hebbar, Arun M. Isloor, Balakrishna Prabhu, Inamuddin, Abdullah M. Asiri, A. F. Ismail, Removal of metal ions and humic acids through polyetherimide membrane with grafted bentonite clay, *Scientific Reports*, 8, 1, (2018), 4665 https://doi.org/10.1038/s41598-018-22837-1

[28] Teuku Rihayat, Suryani, Januar Parlaungan Siregar, Satrianananda, M. Yunus, Sariadi, Fitria, Shafira Riskina, Zuhra Amalia, Wildan Syahputra, Nurhanifa, Safari, Nurul fitriah, Mardani, Jamiluddin Jaafar, Synthesis and Characterization of North Aceh CEC Bentonite Determination with Methylene Blue Method and Increased D-Spacing after Addition of Surfactants CTAB-SDS, *IOP Conference Series: Materials Science and Engineering*, 506, 1, (2019), 012054 https://doi.org/10.1088/1757-899X/506/1/012054

[29] Francine Bertella, Sibele B. C. Pergher, Pillaring of bentonite clay with Al and Co, *Microporous and Mesoporous Materials*, 201, (2015), 116-123 https://doi.org/10.1016/j.micromeso.2014.09.013

[30] Mustapha Lamrani, Mohamed Mouchane, Hanan Taybi, Abdeslam Mouadili, Comprehensive Review on the Adsorption Properties of Clay Minerals for Enhanced Removal of Toxic Dyes and Heavy Metals, *Journal of Water and Environmental Nanotechnology*, 10, 1, (2025), 85-107 https://doi.org/10.22090/jwent.2025.01.08

[31] Tamas Szabo, Plinio Maroni, Istvan Szilagyi, Size-dependent aggregation of graphene oxide, *Carbon*, 160, (2020), 145-155 https://doi.org/10.1016/j.carbon.2020.01.022

[32] Iona M. McIntosh, Alexander R. L. Nichols, Kenichiro Tani, Edward W. Llewellin, Accounting for the species-dependence of the 3500 cm^{-1} H_2O_t infrared molar absorptivity coefficient: Implications for hydrated volcanic glasses, *American Mineralogist*, 102, 8, (2017), 1677-1689 https://doi.org/10.2138/am-2017-5952CCBY

[33] Ángel David Gálvez-Serna, Iván Fernando Macías-Quiroga, Gloria Inés Giraldo-Gómez, María Teresa Dávila-Arias, Nancy Rocío Sanabria-González, Catalytic Oxidation of Tartrazine in Aqueous Solution Using a Pillared Clay with Aluminum and Iron, *Bulletin of Chemical Reaction Engineering & Catalysis*, (2021), 76-87 https://doi.org/10.9767/bcrec.16.1.9978.76-87

[34] Desnelli, W. R. Asri, Hasanudin, M. Said, P. L. Hariani, Removal of Congo Red and Procion Red Using Zn/Fe Pillared Bentonite, *IOP Conference Series: Earth and Environmental Science*, 926, 1, (2021), 012051 https://doi.org/10.1088/1755-1315/926/1/012051

[35] Muhammad Nauval Farras Russamsi, Firman Joshua Nainggolan, Triati Dewi Kencana Wungu, Suprijadi, Carbon Dioxide Adsorption on Iron (III) Oxide Pillarized Na-Montmorillonite, *Sains Malaysiana*, 53, 2, (2024), 409-419 http://doi.org/10.17576/jsm-2024-5302-14

[36] Sisnayati Sisnayati, Muhammad Said, Nabila Aprianti, Ria Komala, Hendra Dwipayana, Muhammad Faizal, Metal Pillared Bentonite Synthesis and its Characteristics Using X-Ray Diffraction, *Journal of Ecological Engineering*, 23, 12, (2022), 68-74 https://doi.org/10.12911/22998993/155081

[37] Paul S. Bagus, Connie J. Nelin, C. R. Brundle, N. Lahiri, Eugene S. Ilton, Kevin M. Rosso, Analysis of the Fe 2p XPS for hematite α Fe_2O_3: Consequences of covalent bonding and orbital splittings on multiplet splittings, *The Journal of Chemical Physics*, 152, 1, (2020), 014704 https://doi.org/10.1063/1.5135595

[38] Carlos Mota-Heredia, Jaime Cuevas, Raúl Fernández, Effect of Iron Chloride (II) on Bentonites under Hydrothermal Gradients: A Comparative Study between Sodium Bentonite and Calcium Bentonite, *Minerals*, 14, 2, (2024), 132 https://doi.org/10.3390/min14020132

[39] Dong Wan, Guanghua Wang, Wenbing Li, Xiaobi Wei, Investigation into the morphology and structure of magnetic bentonite nanocomposites with their catalytic activity, *Applied Surface Science*, 413, (2017), 398-407 https://doi.org/10.1016/j.apsusc.2017.03.265

[40] Negin Nasseh, Lobat Taghavi, Behnam Barikbin, Mohammad Ali Nasseri, Ali Allahresani, $FeNi_3/SiO_2$ magnetic nanocomposite as an efficient and recyclable heterogeneous fenton-like catalyst for the oxidation of metronidazole in neutral environments: Adsorption and degradation studies, *Composites Part B: Engineering*, 166, (2019), 328-340 https://doi.org/10.1016/j.compositesb.2018.11.112

[41] Masayuki Kawaguchi, Akihiro Kurasaki, Intercalation of magnesium into a graphite-like layered material of composition BC_2N, *Chemical Communications*, 48, 55, (2012), 6897-6899 https://doi.org/10.1039/c2cc31435e

[42] Haiyan Li, Dongxiang Liu, Jiyou Chen, Jianping Zhu, Peng Han, Effects of amino alcohols-intercalated MgAl-LDH nanocomposites on the properties of sulfoaluminate cement-based materials, *Construction and Building Materials*, 452, (2024), 138982 https://doi.org/10.1016/j.conbuildmat.2024.138982